行政院國家科學委員會補助專題研究計畫 ■成果報告 □期中進度報告

閘極局域的開放式量子點與一維窄通道的抽運傳輸、整流、與自旋極化機制

計畫類別：■個別型計畫　　□整合型計畫

計畫編號：NSC96－2112－M－009－030－MY3

執行期間：96 年 8 月 1 日至　99 年 11 月 30 日

執行機構及系所：國立交通大學電子物理系

計畫主持人：許世英

計畫參與人員：鍾廷翊（博士,98 畢），劉凱銘（博士,100 畢）

　　　　　　　郭昌洋（碩士,97 畢），林欣毅（碩士,98 畢）

　　　　　　　廖碧珊（碩士,99 畢），莊勝豪（碩士,99 畢）

　　　　　　　黃馨慧（碩士班二年級生）

　　　　　　　王惠潔（碩士班二年級生）

　　　　　　　姜智鈞（碩士班二年級生）

　　　　　　　柯昇（學士班四年級生）

成果報告類型(依經費核定清單規定繳交)：□精簡報告　■完整報告

本計畫除繳交成果報告外，另須繳交以下出國心得報告：

□赴國外出差或研習心得報告

□赴大陸地區出差或研習心得報告

■出席國際學術會議心得報告

□國際合作研究計畫國外研究報告

<div align="center">中　華　民　國　99　年　11　月　30　日</div>

行政院國家科學委員會專題研究計畫成果報告

閘極局域的開放式量子點與一維窄通道的抽運傳輸、整流、與自旋極化機制

Quantum pumping, rectification, and spin polarization of gate-confined open quantum dots and 1D channels

一、中文摘要

　　在一系列類一維在彈道傳輸範疇的量子線，長度從類零到數微米(5μm)，我們完成系統性測量源汲偏壓頻譜和探討線長與電子密度對 zero bias anomaly (ZBA)的相關性，雖然不論量子線長度為何在其線性電導都展規律清晰的數個量子平台，我們發現 ZBA 會隨著量子線長度或電子密度減小而被抑制，而溫度與 zero bias 時的線性電導關係遵守 thermal activation 行為，而此關係可延升至某特定溫度 Tc，我們也更進一步發現這截止溫度與 thermal activated 溫度甚至和 ZBA 的偏壓寬度有倍數相依關係，顯示由源汲極偏壓或溫度所造成的電導值下降似乎來自同一物理機制，我們建議電子電子的散射應該可用以解釋 ZBA 的抑制與電導值的降低。在潔淨的量子線清楚地∨觀察道量子化電導與 ZBA，但在探討類一維通道因附近的雜質導致的電性傳輸變化研究上，發現因為此雜質的存在明顯地在其原整齊的階梯電導曲線出現扭曲的階梯或震盪的訊號，同時也在其源汲偏壓電導能譜上出現複雜性結構，能譜圖展現出雙峰結構且會隨著雜質的分佈而又變成單峰結構，此很容易地與之前探討的 ZBA 混淆，但因為環境因素很容易影響雜質對通道的相關傳輸，所以只要留意針對通道做些環境變化是可以釐清雜質的效應；要研究 ZBA 的特質是先要有一沒有雜質影響的類一維通道。

關鍵詞：閘極局域量子線、0.7 結構、熱激發行為、微分電導能譜。

Abstract

　　We present a systematic study on the zero-bias conductance peak and its dependences on the carrier density and structural geometry in quasi-one-dimensional quantum wires (QWs). This zero-bias anomaly (ZBA) is suppressed by either decreasing the carrier density or increasing the QW length. The differential conductance at zero bias decreases with increasing temperature in accordance with a thermal-activation model up to a well-defined cut-off temperature. We demonstrate that the activation energy, cut-off temperature, and width of the ZBA are correlated, and suggest that these features are controlled by electron scattering in QWs. Conductance quantization and the zero bias anomaly (ZBA) are robust in clean QWs. In contrast, disordered QWs show complexities in the ways of onductance resonance, peak splitting and trace crossing in source–drain bias spectroscopies. The experimental results and theoretical predictions are in congruence. Moreover, the resonant state arising from the impurities results in either a single peak or double-splitting peaks in the spectroscopies from the detailed impurity configurations. The resonant splitting peaks are found to influence the ZBA, indicating that a clean QW is crucial for investigating the intrinsic characteristics of the ZBA of QWs.

Keywords: gate-confined quantum wire, the 0.7 structure, thermal activated behavior, differential conductance spectroscopy.

二、緣由與目的

In a ballistic quasi-one-dimensional (1D) channel, the linear conductance is quantized into integer multiples of $G_o=2e^2/h$ due to the transmission of spin-degenerate 1D subbands within a noninteracting electron picture.[1,2] Peculiar phenomena, however, such as a 0.7 anomaly and a zero-bias Anomaly (ZBA), referred to as the conductance peak centered at zero bias in source-drain bias spectroscopy, are often observed near the first quantization plateau and have attracted much attention.[3,4] The 0.7 anomaly which usually accompanies a conductance reduction near the first plateau, a lowered conductance at high temperatures, was mostly attributed to spin-related mechanisms.[4–20] One-dimensional Kondo physics was proposed to describe the experimental findings, such as the scaling of conductance to a modified Kondo form and the splitting of a zero-bias conductance peak in a parallel magnetic field.[4,17–20] More recently, however, others have claimed that 1D Kondo physics does not fully explain the intricate behaviors of the ZBA.[21–23] In some devices, the splitting of a zero-bias conductance peak is absent in magnetic fields as high as 10 T and at $G<0.5G_o$, where the channel is fully spin-polarized.[22] In a few devices, splitting occurs in magnetic fields but two split peaks can resolve back into a single peak by laterally shifting the quantum wire(QW).[22,23] Additionally, zero-bias conductance peak splitting is almost linearly dependent on the split gate voltage.[23] These findings indicate that ZBA cannot be explained by Kondo physics. Thus, the issue is not yet completely clarified and a comprehensive understanding requires further study.

三、實驗方法

The two dimensional electron gas(2DEG) which forms at the interface of an Al$_x$Ga$_{1-x}$As/GaAs heterostructure was grown using MBE by Dr. Umansky at Wiezmann institute in Israel. Shubnikov-de Haas and Hall measurements were used to determine the areal electron density n. Mobility μ is about 2.2×10^6 cm^2/Vs and n is 1.4×10^{11}cm^{-2} corresponding to the elastic mean free path ℓ of ~15μm at low temperatures.

Electron beam lithography along with thermal deposition were used to fabricate metallic gates on (100) plane of the substrate. A quasi-onedimensional quantum wire can be formed by depleting the 2DEG ~93 nm beneath the negatively biased split gate pair. The length of our QWs ranges from quasi-zero to 5μm while the nominal gap width is kept constant at ~0.45μm. A metallic top gate (tp) was fabricated on top of the split gates, isolated by a ~100-nm-thick dielectric layer of cross-linked polymethylmethacrylate, to control the carrier concentration. Measurements were performed mainly in a pumped ^{3}He cryostat and occasionally in a dilution refrigerator with base temperatures of 0.27 K and 40 mK, respectively. Differential conductance ($G = \dfrac{\partial I}{\partial V_{sd}}$) measurement was carried out using a standard four probes ac lock-in technique at 51 Hz with a

To control the position of the QWs and impose various impurity configurations, the split gates were offset by a voltage bias, ΔV_g. Without being mentioned throughout the paper, $V_g +1/2\Delta V_g$ was applied on one gate and $V_g -1/2\Delta V_g$ was applied on the other. The position displacement is linearly dependent with ΔV_g [24, 25].

四、實驗結果

When the negative voltage is applied to a pair of split gates, the potential depletes 2DEG to form the quasi-1D channel resulting in the typical quantized conductance. As shown in Fig. 1, there are conductance plateaus in units of 2e^2/h due to the

transmission of 1D sub-bands for a L=0.45μm QW. As known, 1D transport is sensitive to the carrier density which can be effectively tuned by biasing top gate voltage V_{tg}. The more negative V_{tg} is, the less carrier density n is. The more positive V_{tg} is, the more carrier density n is. Quantized conductance for a series of V_{tg} is also demonstrated in Fig. 1. The carrier density is smoothly decreased from left to right corresponding to that the threshold V_{sg} for pinching off becomes less negative continuously. The number of plateau is determined by the number of sub-band with energy less than Fermi energy E_F. As seen in the inset of Fig. 1, the reduction of V_{tg} leads to the decrease of the observed plateau number implying the decrease of E_F. Besides, when carrier density is large, the conductance plateaus are much clear. Once carrier density is severely reduced, the plateau disappears.
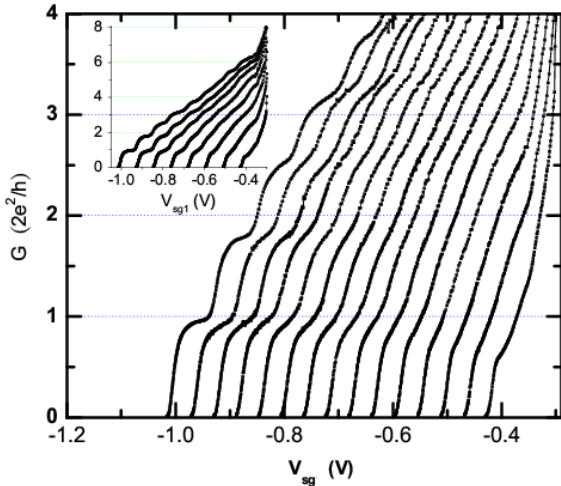

Fig. 1 Quantized conductance of the L=0.45μm QW as a function of split gate voltage at T=0.3K for different top gate voltages. From left to right: V_{tg} decreases from +0.4V to -1V in a step of 0.1V Inset: selected data curves are shown in the large y-scale.

It has been well known that the carrier density depends on V_{tp} in heterostructures no matter in either 1D or 2D [10]. Fermi energy is determined by carrier density and dimensionality following that $E_F = \pi^2 \hbar^2 n_{1D}^2 / 8m^*$ in 1D and $E_F = \pi n_{2D} / 2m^*$ in 2D where n_{1D} and n_{2D} are

carrier densities in 1D and 2D, respectively. m^* is the effective mass of carrier. Here, the transconductance-source drain voltage V_{sd} characteristic referred as the half-plateau method based on Glazman and Khaetskii model[27] is used to obtain the sub-band energy level spacing and corresponding Fermi energy [28]. Both V_{tg} calculated carrier densities versus V_{tg} in 1D and 2D models are plotted in Fig. 2. As seen, carrier density is indeed effectively changed by tuning V_{tg}.
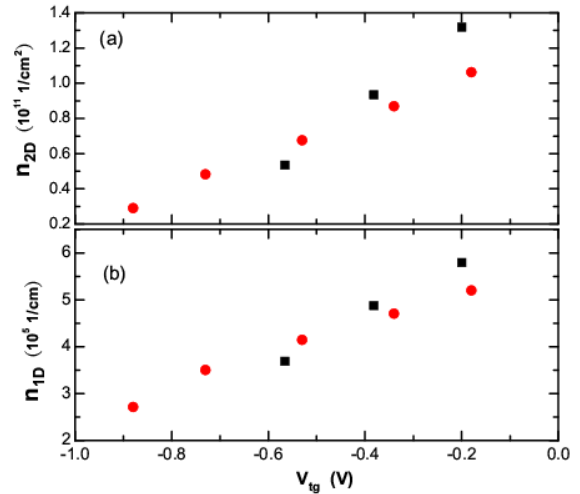

Fig. 2 (Top) Calculated two dimensional carrier density and (Bottom) calculated one dimensional carrier density versus top gate voltage for the L=0.45μm QW. Sub-band index of the QW is confined at N=4 (black squares) and N=6 (red circles), respectively.

By sweeping dc source-drain voltage V_{sd} across a confined QW and measuring the dynamic conductance $G=dI/dV_{sd}$, the source-drain bias spectroscopy was investigated. Figs.3 (a)-(c) show source-drain bias spectroscopies $G(V_{sd})$ against V_{sg} of the sample in Fig.3 for identical top gate voltages at T=0.3K. The ZBA characteristic is often expected. For V_{tp}=+0.4V in Fig.3(a), the differential conductance exhibits a clear peak at zero bias forming ZBA distinctive to the bell shaped structure contributed from non-equilibrium transport of sub-bands for $G<G_o$. From source-drain bias spectroscopies of numerous samples at a series of V_{tp}, we find that ZBA becomes weaker with

decreasing carrier density. As shown in Figs.3(b) and 3(c), ZBA is narrower in width for $V_{tp}=-0.1V$ and disappears for $V_{tp}=-1.45V$. Here, we characterize the width of ZBA by ΔV_{sd}^{ZBA}, the source-drain voltage difference between the 'peak' and 'bottom' of ZBA. In Fig.3(a), the width decreases from ~750μV (the red trace labeled by a star) to ~280μV (the blue trace labeled by a solid circle)with decreasing V_{sg}. ZBA is absent for $V_{sg}<-986mV$. In Fig.3(b), the ZBA width decreases from ~250μV (the red trace labeled by a star) to ~160μV (the blue trace labeled by a solid circle)with decreasing V_{sg}. ZBA is absent for $V_{sg}<-891mV$. As to the lowest carrier density sample in Fig.3(c), no ZBA is present for all split gate voltages. Therefore, ZBA is suppressed by decreasing carrier density. The systematic observation is in consistence with the other report by Reilly *et al.*.[12] The authors suggested that carrier density induced enhancement in spin splitting results in a strong ZBA. On the other hand, the scenario may be attributed to electron-electron interactions (EEI).
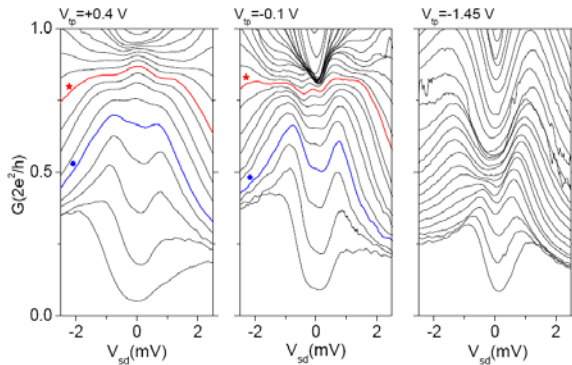

Fig. 3 Source-drain bias spectroscopies at 0.3K of the L=0.5μm quantum wire for (a)$V_{tp}=+0.4V$, (b) $V_{tp}=-0.1V$, and (c) $V_{tp}=-1.45V$, respectively at various V_{sg}. (a) V_{sg} ranges from −938 to −994mV in steps of 4mV. (b) V_{sg} ranges from −819 to −897mV in steps of 3mV. (c) V_{sg} ranges from −280 to −324mV in steps of 2mV.

The temperature dependence of the 0.7 structure has been intensely studied for a while, however the results are quite diverse. Among them two types are mostly be proposed, the Kondo-like and an activated temperature dependences. As mentioned above, our samples with very low carrier density demonstrate a nearly temperature-insensitive conductance in the temperature range from 0.28K to 2K. While increasing V_{tp} (n), conductance indeed depends on temperature. We plot three G(T) traces of a quasi-zero QW in the inset of Fig.4 to show the typical temperature dependent conductance behavior. Differential conductance at zero bias decreases with increasing temperature. Numerical fits using both Kondo-like[4] and thermal activation models to data in the inset of Fig.4 are shown as dotted and solid lines, respectively. Both models seem describe experimental results well at low temperatures. However, the applicable temperature range is wider and the fitting parameter obtained from the fit exhibits a systematic variation in the activation model. Hence, we adopt the activation model to analyze data.

In order to compare with the theoretical prediction, we fit the data with a modified formula, where G(0) is the measured conductance at the base temperature. T_a and C are the fitting parameters.[6] Rearranging the equation, f_a defined as $\dfrac{1}{C}\left(1-\dfrac{G(T)}{G(0)}\right)$ equals to $e^{-T_a/T}$. Semilogarithmic plots of f_s versus 1/T are presented to confirm such typical activated behavior. Semilogarithmic plots of f_a versus T_a/T for a quasi-zero QW against a series of V_{sg} at $V_{tp}=0$ are presented in Fig.4 to confirm such typical thermal activation behavior. As seen, all traces after scaling T by T_a in this semilogarithmic Arrhenius plot generally collapse onto an universal curve following a linear relation up to around $0.1T_a$. The dashed line is the least square root linear fit. Thermal activation behavior is seen to be valid up to a ``cutoff'' temperature, $T_c$. In Fig.4, many traces of $f_a$ show a downward trend deviating from the linear fit at low values of $T_a/T$. $T_c$ can be easily determined by the fit. As shown in the inset of Fig.4, the ``cutoff'' temperature, T_c, for

each V_{sg} is labeled. The evolution of T_c with either V_{sg} or G(0) is obtained for G<G_o. As G(0) decreases, T_c decreases and so does T_a. In addition, T_a depends on the split gate voltage and increases from sub-Kelvin near $0.5G_o$ to a few kelvin in the proximity of the first plateau. Other samples except those with either low carrier density or long channel length have the similar behavior exhibiting an exponential dependence of the activation energy on split gate voltage in consistence with experimental findings by other groups.[21,22] It has been proposed by Bruus *et al.* that the observed activated behavior in G is related to the thermal depopulation of a subband with a gate-voltage dependent subband edge.[29] Power law relation between the activation energy and split gate voltage was experimentally obtained by Bruus *et al.*.[30,31]
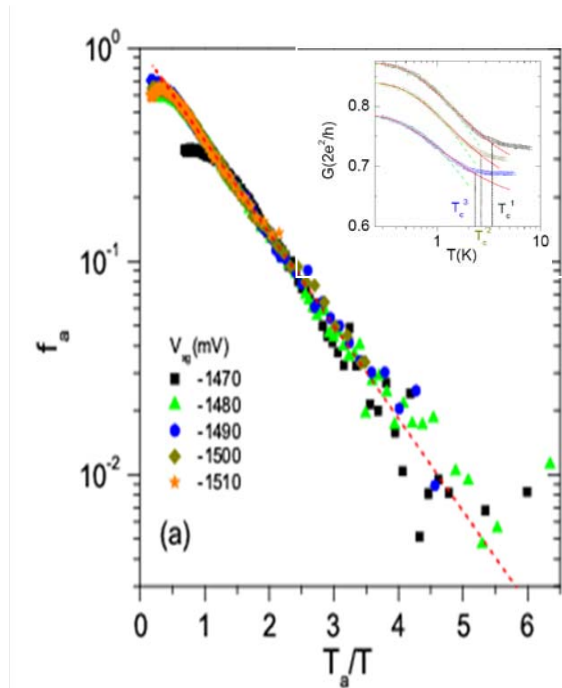

Fig. 4 Semilogarithmic plot of f_s versus T^{-1} for sample C with (a) V_{top}=0V and V_{top}=−0.6V, respectively. Points are the experimental data and lines are the linear fits. Inset: Linear plot of one data G(T). Inset: Three typical traces of measured G(T), along with the simulated curves of activation model(solid lines) and Kondo-like model(dotted lines)\cite{note}. The cutoff temperature that G(T) deviates from activation behavior is located and indexed as T_c for split voltage V_{sg}.

Furthermore, it is quite interesting to explore that there is not only a correlation between T_a and T_c, but also a close relation between them and ZBA width for G<$0.9G_o$. The relation can be clearly demonstrated by scaling (G(0), T_c), (G(0), T_a) extracted from temperature dependent conductance and (G^{ZBA}_{peak}, ΔV^{ZBA}_{sd}) extracted from source-drain bias conductance spectroscopy on the same plot as shown in Figs.5(a) and 5(b) for two quasi-zero QWs. G^{ZBA}_{peak} is the conductance at the ZBA peak at the base temperature. In Fig.5(a), three traces of (G(0), $2k_BT_c$), (G(0), 5.5 k_BT_a), and (G^{ZBA}_{peak}, ΔV^{ZBA}_{sd}) collapse onto one curve. Similarly in Fig.5(b), three traces of (G(0), $3k_BT_c$), (G(0), 7 k_BT_a), and (G^{ZBA}_{peak}, ΔV^{ZBA}_{sd}) collapse also onto one curve. Although the factors are slightly different, the scenario is robust. Tc, Ta, and ΔV^{ZBA}_{sd} decrease monotonically with decreasing differential conductance at zero bias. The result confirms that the temperature induced conductance reduction is indeed associated with ZBA in nonlinear conductance spectroscopy. In consistence with other data, the absence of ZBA is usually accompanied with temperature insensitive conductance for G<G_o in QWs with low carrier density.
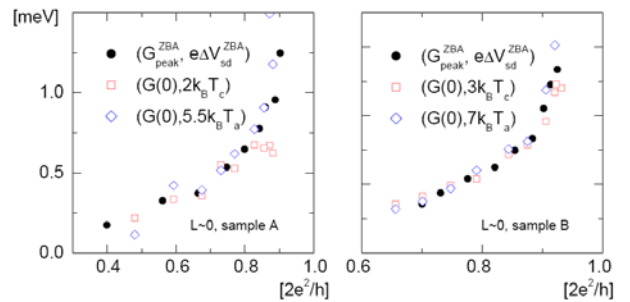

Fig. 5 (G^{ZBA}_{peak}, eΔV^{ZBA}_{sd}), (G(0), scaled k_BT_c), and (G(0), scaled k_BT_a) on the same measures for two quantum wires of quasi-zero length.

The match of three traces obtained from two different measurements suggests that the conductance reductions at finite temperatures

and at finite biases are strongly correlated.

Here, we provide evidence that ZBA depends systematically on physical properties of QWs. The amplitude and width of the ZBA decrease with either decreasing carrier density or increasing channel length, wherein the scattering rate of electrons is expected to increase. The ZBA is totally suppressed by strong scattering, in a either very low carrier density or long QW. The activation model is preferable for describing the temperature-dependent conductance reduction. Moreover, the conductance dependence on temperature departs from the activation model at a cutoff. Scaling of the cut-off energy, activation energy, and ZBA width indicates that the temperature- and bias-induced conductance reductions are affected by the same physics. Theoretical predictions taking electron backscattering into account are in accordance with our results. We believe that electron scattering play a central role in our observations.

. We also made comparisons of linear conductance and source–drain bias spectroscopy between clean and disordered QWs. We particularly adopted a lateral shifting technique to systematically vary the impurity configurations in disordered QWs. Laterally shifting the QWs by independently biasing the split gate voltage implies spatial displacement of the confined 1D channel with an asymmetrically confining potential, which was supported by theoretical calculations [24, 25].

When both split gates are applied to the same negative voltage, the confining potential of the QW is transversely symmetric and the transport is a typically quantized conductance behavior. By differentially biasing both gates by ΔV_g, $V_g + 1/2 \Delta V_g$ being applied on one gate (right) and $V_g - 1/2 \Delta V_g$ being applied on the other gate (left), the confining potential becomes asymmetric and conductance traces may evolve differently. We found that conductance traces in two separate cooling processes reveal non-oscillating conductance and clear quantization steps without

distortions, implying that the sample is less disordered. In general, the linear conductance of a clean QW of quasi-zero length is robust and reproducible in different cooling processes. Moreover, The ZBA is reproducible after thermal cycling, too.

Figure 6(a) shows conductance traces against a series of ΔV_g. The traces are offset in turn in 50 mV steps for clarity. At $\Delta V_g = 0$, the conductance trace demonstrates more than 14 clear quantization steps. Since the pinch-off voltage remains the same, being independent of ΔV_g, the plotted traces are certainly uniformly spaced at 50 mV spacing for the artificial offset. A slight conductance oscillation appears at the sixth and seventh steps for $\Delta V_g = +0.2$ and $+0.4$ V. Except for this small disturbance, the conductance quantization remains unaltered with respect to the lateral shifting, confirming that the device is quite clean. Figures 6(b) and (c) show the spectroscopies of the QW at two opposite conditions, $\Delta V_g = +0.6$ and -0.6 V. The QW is shifted from one side to the other relative to the symmetrical confinement at $\Delta V_g = 0$. Both figures demonstrate ZBA for $G < G_o$. The ZBA is slightly weaker in figure 6(b).
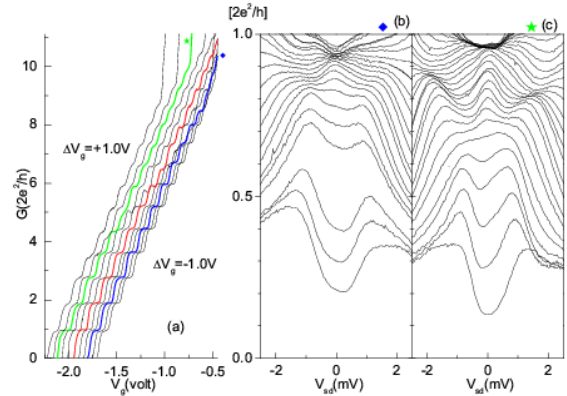

Fig. 6 (a) $G(V_g)$ of the clean quantum wire against the differential voltage difference _Vg. (See text) From left to right, $\Delta V_g = +1.0 \sim -1.0$ V in 0.2 V steps. The traces are offset in turn by 50 mV for clarity. The middle red line is for $\Delta V_g = 0$. (b)–(c) Source–drain bias spectroscopies for $\Delta V_g = -0.6$ and $+0.6$ V, respectively. (b) $V_g = -1.846 \sim -1.934$ V in 4 mV steps. (c) $V_g = -1.848 \sim -1.964$ V in 4 mV steps.

In figure 7(a) we also plot other conductance traces of a disordered QW against a series of $\Delta \tilde{V}g$, from +0.5 to −0.5 V in 0.1 V steps. The middle red line labeled by a triangle is an example that the confining potential of the QW is transversely symmetric and the transport is expected to be a typically quantized conductance behavior. However, weak conductance oscillations are discernible along the conductance trace besides the five conductance plateaus. By differentially biasing both gates by $\Delta \tilde{V}g$, V_g being applied on one gate (right) and $V_g + \Delta \tilde{V}g$ being applied on the other gate (left), the confining potential becomes asymmetric and conductance traces evolve differently. Figure 7(b) displays the scanning electron microscopic (SEM) image of both gates. The QW is monotonically shifted with $\Delta \tilde{V}g$. The pinch-off voltage decreases (becomes more negative) with increasing $\Delta \tilde{V}g$. The electron path is shifted slightly towards the right for a negative $\Delta \tilde{V}g$ while it shifts to the left for a positive $\Delta \tilde{V}g$. As seen in figure 7(a), the number of plateaus is reduced by the asymmetrical confining potential. The confining potential is higher and steeper for the more negatively biased gate while being lower and smoother for the other less negatively biased gate. A strong resonant peak emerges by shifting the QW to the right (lowering the confining potential at the right-hand side) for $\Delta \tilde{V}g \leq −0.1$ V, while the peak conductance tends to pin at $0.5G_o$. Notice that the superimposing resonances are stronger for the negative $\Delta \tilde{V}g$ regime.
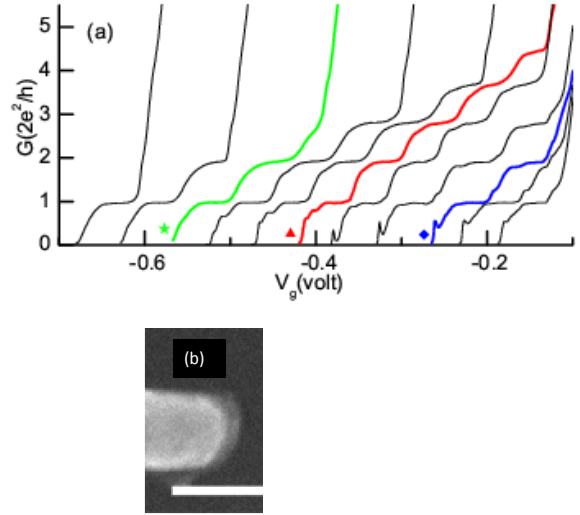

Fig.7 (a) $G(V_g)$ against $\Delta \tilde{V}g$ of a disordered QW in the presence of strong conductance oscillations at 0.3 K. $\Delta \tilde{V}g$ = +0.5 (leftmost) and −0.5 V (rightmost) in 0.1 V steps. (b) Micrograph of the disordered QW. The scale bar has a length of 0.4μm. V_g is applied on the right gate and $V_g + \Delta \tilde{V}g$ is applied on the left gate.

The effect of the resonances on the source–drain bias spectroscopy is presented in figure 8 (top panel) for three $\Delta \tilde{V}g$. The ZBA, conductance peak at $V_{sd} = 0$, is seen in all three spectroscopies for $G < G_o$ coexisting with the splitting peaks at nonzero V_{sd}. For instance, two strong satellite peaks appear at the sides of the ZBA at $|V_{sd}| \sim 0.8$ mV on the dot-labeled curve of $V_g = −383$ mV in figure 8 (c). Similar phenomena have been reported by Sfigakis *et al.* for dot-coupled QWs [21]. The concurrence of the ZBA and resonant peaks forming a triple-peak structure can be attributed to the resonant states. The characteristics of the ZBA, i.e. the amplitude and width of the conductance peak, are affected by the resonant peaks. The satellite peaks appear at larger $|V_{sd}|$ for an asymmetric confining potential, e.g. at ~1.9 mV in figure 8(a) of $\Delta \tilde{V}g = +0.3$ V, and at ~1.8 mV in figure 8(c) of $\Delta \tilde{V}g = −0.3$ V for the dot-labeled curves. Compared with figures 8(a) and (c), the ZBA is weaker and suppressed more rapidly with decreasing V_g for a symmetric confining potential ($\Delta \tilde{V}g=0$) as shown in figure 8(b). The results indicate that the existence of the

resonant peaks due to the resonant states near the $V_{sd} = 0$ suppresses the ZBA. The evolution of the split peaks with respect to Vg, indicated by the dashed lines in figure 8(b), resembles the diamond structure of the tunneling spectroscopy of zero-dimensional states. A similar evolution of the satellite peaks is also observable in figure 8(b) in both conductance ranges, $G < G_o$ and $G_o < G < 1.75G_o$, for the higher subband.
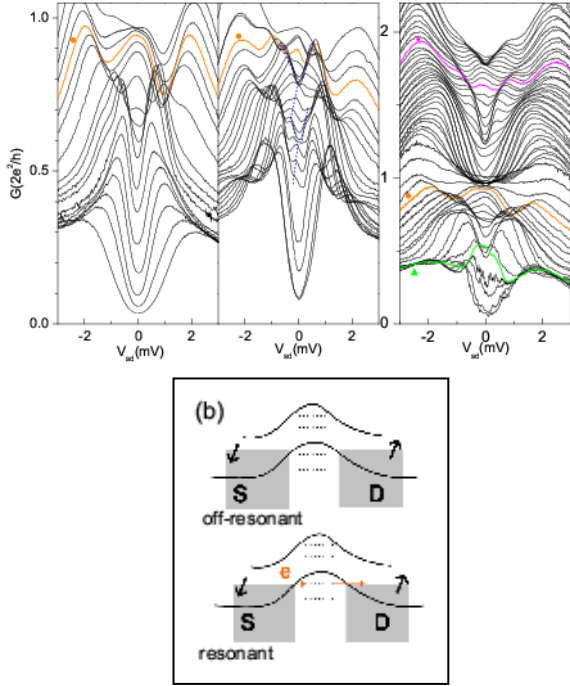

Fig.8. (Top) Source–drain bias spectroscopies for various $\Delta\tilde{V}g$. (a) +0.3V, (b) 0 V and (c) −0.3 V. Dashed lines are visual guides for the evolution of conductance peaks as a function of V_g and V_{sd}. (Bottom) Scenario for the splitting peaks in source–drain bias spectroscopies. The thick lines stand for the last two subbands of a QW while the dotted lines stand for the resonant levels induced by impurities.

The triple-peak structure appears also at the higher conductance regime for $1.55G_o < G < 1.75G_o$ at $\Delta\tilde{V}g = -0.3$ V as shown in figure 8(c). The central peak in this range is weaker compared with the strong *single* peak observed in the same conductance range in the clean QW (see the following paragraphs). The appearance of the central peak at such a high conductance regime implies that the ZBA is not unique for the low conductance regime on which most research groups focused. Although there is no resonance in the linear conductance trace for $\Delta\tilde{V}g = +0.3$ V, groups of crossed traces appear in all three graphs, indicating strong conductance resonances in the finite V_{sd} regime. Available levels of a QW in the presence of resonant states induced by impurities are depicted in figure 8 (bottom panel). Thick and dotted lines represent the last two subbands and impurity-induced resonant levels, respectively. Alignment of a resonant level with the chemical potential of either source or drain increases the transmission probability or the differential conductance G. The mechanism is analogous to the resonant tunneling in a quantum dot. Finite V_{sd} would be required to align the chemical potential with a resonant state when the QW is not initially in resonance, resulting in the evolution of splitting peaks with respect to V_{sg} in spectroscopy and conductance resonances at finite V_{sd}. Although this is an oversimplified scenario, it provides a qualitatively suitable explanation for our results. Additionally, when the QW is shifted by $\Delta\tilde{V}g$, the relative position of the impurity is changed as well as the details of the resonant state. As expected, figures 8(a)–(c) present different curve structures for these three $\Delta\tilde{V}g$.

We have studied the linear conductance and source–drain bias spectroscopies of clean and disordered quantum wires (QWs) against thermal cycling and lateral shifting, which change the impurity configuration. Conductance quantization and the zero bias anomaly (ZBA) are robust in clean QWs. In contrast, disordered QWs show complexities in the ways of conductance resonance, peak splitting and trace crossing in source–drain bias spectroscopies. The experimental results and theoretical predictions are in congruence. Moreover, the resonant state arising from the impurities results in either a single peak or double-splitting peaks in the spectroscopies from the detailed impurity configurations. The resonant splitting peaks are found to influence the ZBA, indicating that a clean QW is crucial for investigating the intrinsic characteristics of the ZBA of QWs.

四、結論

In summary, we provide evidence that ZBA depends systematically on physical properties of QWs. The amplitude and width of the ZBA decrease with either decreasing carrier density or increasing channel length, wherein the scattering rate of electrons is expected to increase. The ZBA is totally suppressed by strong scattering, in a either very low carrier density or long QW. The activation model is preferable for describing the temperature-dependent conductance reduction. Moreover, the conductance dependence on temperature departs from the activation model at a cutoff. Scaling of the cut-off energy, activation energy, and ZBA width indicates that the temperature- and bias-induced conductance reductions are affected by the same physics. Theoretical predictions taking electron backscattering into account are in accordance with our results. We believe that electron scattering play a central role in our observations.

ZBA is robust in clean short QWs against lateral shifting and thermal cycling. On the other hand, impurities can cause resonances leading to the complicated source–drain spectroscopies. These resonant features are sensitive to thermal cycling and lateral shifting of QWs, revealing the random nature of impurities in ballistic QWs. The double-split peaks due to resonant levels affect the characteristics of ZBA. The results indicate that cleanliness (impurity-free) is crucial for studying the intrinsic behaviors of ZBA in one-dimensional systems.

五、參考文獻

1. D. A. Wharam, T. J. Thornton, R. Newbury, M. Pepper, H. Ahmed, J. E. F. Frost, D. G. Hasko, D. C. Peacock, D. A. Ritchie, and G. A. C. Jones, J. Phys. C **21**, L209 (1988).
2. B. J. van Wees, H. van Houten, C. W. J. Beenakker, J. G. Williamson, L. P. Kouwenhoven, D. van der Marel, and C. T. Foxon, Phys. Rev. Lett. **60**, 848 (1988).
3. K. J. Thomas, J. T. Nicholls, M. Y. Simmons, M. Pepper, D. R. Mace, and D. A. Ritchie, Phys. Rev. Lett. **77**, 135 (1996).
4. S. M. Cronenwett, H. J. Lynch, D. Goldhaber-Gordon, L. P. Kouwenhoven, C. M. Marcus, K. Hirose, N. S. Wingreen, and V. Umansky, Phys. Rev. Lett. **88**, 226805 (2002).
5. R. Akis and D. K. Ferry, J. Phys.: Condens. Matter **20**, 164201 (2008).
6. A. Starikov, I. I. Yakimenko, and K. F. Berggren, Phys. Rev.B **67**, 235319 (2003).
7. K. F. Berggren and I. I. Yakimenko, Phys. Rev. B **66**, 085323 (2002).
8. P. Jaksch, I. Yakimenko, and K. F. Berggren, Phys. Rev. B **74**, 235320 (2006).
9. Lassl, P. Schlagheck, and K. Richter, Phys. Rev. B **75**, 045346 (2007).
10. P. Havu, M. J. Puska, R. M. Nieminen, and V. Havu, Phys. Rev. B **70**, 233308 (2004).
11. D. J. Reilly, G. R. Facer, A. S. Dzurak, B. E. Kane, P. J. Stiles, R. G. Clark, A. R. Hamilton, J. L. O'Brien, N. E. Lumpkin, L. N. Pfeiffer, and K. W. West, Phys. Rev. B **63**, 121311(R) (2001).
12. D. J. Reilly, T. M. Buehler, J. L. O'Brien, A. R. Hamilton, A. S. Dzurak, R. G. Clark, B. E. Kane, L. N. Pfeiffer, and K. W. West, Phys. Rev. Lett. **89**, 246801 (2002).
13. D. J. Reilly, Phys. Rev. B **72**, 033309 (2005).

14. Y. Tokura and A. Khaetskii, Physica E **12**, 711 (2002).

15. K. A. Matveev, Phys. Rev. B **70**, 245319 (2004).

16. K. A. Matveev, Phys. Rev. Lett. **92**, 106801 (2004).

17. Y. Meir, K. Hirose, and N. S. Wingreen, Phys. Rev. Lett. **89**, 196802 (2002).

18. K. Hirose, Y. Meir, and N. S. Wingreen, Phys. Rev. Lett. **90**, 026804 (2003).

19. T. Rejec and Y. Meir, Nature (London) **442**, 900 (2006).

20. J. H. Hsiao, K. M. Liu, S. Y. Hsu, and T. M. Hong, Phys. Rev. B **79**, 033304 (2009).

21. F. Sfigakis, C. J. B. Ford, M. Pepper, M. Kataoka, D. A. Ritchie, and M. Y. Simmons, Phys. Rev. Lett. **100**, 026807 (2008).

22. T. M. Chen, A. C. Graham, M. Pepper, I. Farrer, and D. A. Ritchie, Phys. Rev. B **79**, 153303 (2009).

23. S. Sarkozy, F. Sfigakis, K. Das Gupta, I. Farrer, D. A. Ritchie, G. A. C. Jones, and M. Pepper, Phys. Rev. B **79**, 161307(R) (2009).

24. F. Wakaya, J. Takahara, S. Takaoka, K. Murase, and Gamo, Japan. J. Appl. Phys. **35** 1329 (1996).

25. L.I. Glazman and I.A. Larkin, Semicond. Sci. Technol. **6** 32 (1991).

26. B.E. Kane, G.R. Facer, A.S. Dzurak, N.E. Lumpkin, R.G. Clark, L.N. Pfeiffer, and K.W. West, Appl. Phys. Lett. **72**, 3506 (1998).

27. L.I. Glazman and A.V. Khaetskii, Europhys. Lett. **9**, 263 (1989)

28. N.K. Patel, J.T. Nichrolls, L. Martin-Moreno, M. Pepper, J.E.F. Frost, D.A. Ritchie, and G.A.C. Jones, Phys. Rev. B**44**, 13549 (1991).

29. K. Hirose, S.S. Li, and N. S. Wingreen, Phys. Rev. B **63**, 033315 (2001).

30. A. Kristensen, H. Bruus, A.E. Hansen, J. B. Jensen, P.E. Lindelof, C.J. Marckmann, J. Nygard, C.B. Sorensen, F. Beuscher, A. Forchel, and M. Michel, Phys. Rev. B **62**, 10950 (2000).

31. H. Bruus, V. Cheianov, and K. Flensberg, Physica E **10**, 97 (2001).

國科會補助專題研究計畫項下出席國際學術會議心得報告

計畫編號	NSC 96－2112－M－009－030－MY3		
計畫名稱	閘極局域的開放式量子點與一維窄通道的抽運傳輸、整流、與自旋極化機制		
出國人員姓名	許世英	服務機構及職稱	國立交通大學電子物理系副教授
會議時間	99 年 11 月 13 日 至 99 年 11 月 18 日	會議地點	Atlanta(亞特蘭大),USA(美國)
會議名稱	（中文)第五十五屆美國磁性物理會議 （英文)55th annual conference on magnetism and magnetic materials		
發表論文題目	（中文) （英文)Inhomogeneous magnetization reversal in patterned permalloy planar wires probed by magneto-transport		

一、參加會議經過

11/13 中午搭乘大韓航空從桃園飛首爾班機，在首爾待了約三小時轉大韓 KE033 飛亞特蘭大，長途跋涉，經過層層檢察關卡，總算於晚上 6:30 順利地抵達。只是最後一道入關竟如同出關一樣的檢查程序，教人啞口無言。搭乘地鐵到距離 hotel 最近的 Peachtree center 站，一路上非洲裔乘客眾多，頓時有點感受，出了地鐵，因已近 9:00PM 天色已暗，這城市近似空城般，只有遊民與警察四散街角，走著走著竟然有點害怕，居然走過頭了錯過了 hotel 的 block，最後居然問了路過的三名美籍遊子，憑藉其高科技的 GPS 系統，找到了 200m 外的目的地。Check in 後趕緊拆箱整理，度過平安的一晚。

11/14 由於下午才開始註冊，早上就到 downtown 附近走走，發現這城市高樓大廈四處林立，但周日卻是空蕩蕩、毫無人煙，非洲裔人口多，有些無聊。中午在地鐵站碰到系上王律堯博士與高雄師範大學仁教授，就一起到 Mall 的 Food court 用餐，下午就到在 Hyatt 的會場報到，拿了本周的議程與所有的 abstracts 的 CD，晚上大會備有 reception，就與陸續來報到的朋友聊天用餐，享用美食，飽餐一頓。離開會場竟然下起大雨，幸虧 Hyatt 的門房熱心地贈與小雨傘一把，才免遭落湯雞一劫。回旅館註記了明天該聽的演講與該看的壁報。

11/15 早上出門仍是傾盆大雨，真有些不方便；由於我們的次微米鐵磁平板線的磁電阻研究一直少了微磁動力方程的數值分析解，第一場就趕往 section of micromagnetics and numerical modeling(AH)聽聽這方面的進展；顯然現在有些軟體公司贊助各大學理論數值模擬分析研究團隊發展更快速與大量處理能力的套裝模擬軟體，10:00AM 之後趕至另一 section(AD)聽聽一些"spin injection to metals"相關研究,除了之前熱門的 spin Hall

effect 另一最近的 inverse spin-Hall effect 也仍是持續的研究題材，其實有很大的發展空間作為不需外加磁場下的自旋操控與偵測。11:30AM 結束後，由於尚未熟悉附近環境，就只好在會場所在 Hyatt 大廳販賣部買個三明治果腹，然後就匆忙去看壁報，很多奇奇怪怪的磁性氧化物都具有依些有趣的磁性質，可惜自己實驗室實在無法投入相關研究，出國前問了一些合金材料價格真是不斐，教人不敢領教。下午的 oral 從 1:30PM 就開始了，到 section(BD)凝聽關於"spin injection into semiconductors"，其中居然也包含一 invited talk"二維電子氣 Rashba spin-orbit interaction 所造成的 spin precession"，因為必須 3:00PM 以前就去展示我們的壁報，所以就抽空去行動，隔壁恰好是清大賴老師的學生，提供了一些協助，聽完演講後，就待在壁報前直到 6:00PM。陸續有一些人出現討論，有些是學生或感覺剛入行研究人員，想探詢一些基本磁區翻轉機制與量測，或分享一些自己成果，我覺得目前的數據尚缺模擬的數值分析來佐證，回國之後應該要加緊補足此一欠缺。

11/16 原本預期持續的大雨居然停了，只是仍有些溼冷，但已很感謝了，先去聽了第一場 Domain wall motion 的 invited talk，後又趕去"Magnetic tunnel junctions"的 invited talk，時間真是掌握得宜；今日的早午壁報場壁報時間，參觀幾家廠商，其中一家是設計濺鍍系統的，巧妙精準的設計可以作多用途的製程，而且空間使用非常經濟，一直希望自己實驗室有類似系統，可惜在台灣找不到較精緻手巧且可配合的銲接公司，國外廠商又太昂貴，光是腔體動則上百萬，非小本經營的實驗室所能負荷；也拜訪了美國磁鐵公司(AMI)，他們興奮地展示一個非常小巧的 5Tesla 超導磁鐵，可方便地外掛於低溫系統，另外還可回收液化氦的小規模 dewar，鑒於液氦得越來越高的價位，實在有其需要，只是價格也真不便宜；其實較令人期待的是高溫超導線做的磁鐵。下午聽了 sections DC "Domain wall devices" and DD "Semiconductor devices"的多場演講，其中包含了一些二維電子氣 Rasha interactions。

11/17 早上在壁報會場居然碰到之前在 Michigan state university 作 post doc 時的老闆 Prof. Pratt，幾年前他有受邀來台灣，可惜行程在台北，而我又恰好學校有事沒能接待盡地主之誼；他說已半退休態，雖謙虛地說偶而玩玩實驗，但看起來還是精神抖擻蓄勢待發，對磁性議題永遠有著最大的興致；中午約了仁教授，總算知道原來鄰近的大樓就有個 Food court，人潮擁擠但有著不錯且熱騰騰的中式自助餐。幾天觀察下來，Atlanta 這城市高樓大廈彼間林立，也常有十多層高空中的走廊貫穿兩大樓，白天人聲鼎沸好不熱鬧，但下午五點過後，瞬間人潮退去，整個城市就像個空城，只剩一些遊民與我們這些心裏有些惶恐不安的過客，第一次發現 downtown 僅開的數家便利店，CVS 居然還有警衛駐守，曾在美國遊蕩多年的我從未發現過的事，幾天來的晚上幾乎找不到可用餐遊蕩的地方，只能乖乖地早早回旅館用功。

11/18 今天是議程的最後一天了，早上參與的人很明顯地銳減，有些 section 的聽眾真是寥寥可數，下午沒有壁報展示，所以只有一場 oral section 平均到 4:00PM 左右；因為旅館必須在中午前 check out，所以早上 11:00AM 就趕回去整理行李退房，幾天下來的參與以有些疲累，所以下午找空檔到附近 Olympia 公園與海洋世界走走，晚上就又搭著大韓航空公司的飛機回台灣。(沒料到台灣正為亞運跆拳黑襪事件而抗

韓，不過此時也只有大韓航空的機票最便宜，替政府省荷包考量下只好搭乘)

二、與會心得

在四天緊密的演講-壁報討論節目下，收穫相當多。這次不曉得為什麼有很壁報都未參加，感覺缺席很多，不過參與的人還是很多，歐洲與亞洲參與者占了大多數，反倒美國來的學者相形之下少，也因為會議題材很多元，也多一些材料結構特性分析與應用技術的開發，不僅只於物理學者也多了材料、化學、生科方面學者與業界技術研發人員參與，也因此多增加見聞。出國參與國際會議是最有效，直接的增進新知的方法，免除在資料期刊上查閱上的遺漏，面對面的溝通，也能藉此提供外國學者得知我們的研究成果，使其了解台灣方面於物理研究上的盡力。

三、考察參觀活動(無是項活動者略)

四、建議

感謝國科會給予的經費補助，此行獲益良多。希望學校與國科會能繼續補助國際之學術交流活動。基於氦在地球非常有限的存量，若要從事低溫實驗，設置液化機是刻不容緩的事情，希望學校能配合國科會在校內設置。

五、攜回資料名稱及內容

Program bulletin, abstract CD, reprints, 產品介紹。

六、其他

Inhomogeneous magnetization reversal in patterned permalloy planar wires by magneto-transport

P.S. Liao (廖蓉雯), H.C. Wang (王惠淑),
T. Y. Chung (鍾旋坤), and S. Y. Hsu (許世英)

Department of Electrophysics, National Chiao Tung University,
Hsinchu 30010, Taiwan

NSC98-2112-M-009-030-MY3 and MOE ATU program   Nov. 15, 2010

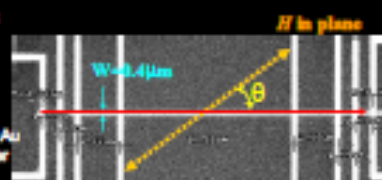電子物理系
NCTU Electrophysics

INTRODUCTION

The ability to fabricate magnetic systems on the sub-micron scale increasingly produces new physical phenomena and poses challenges to established models of magnetic behavior. The geometry as well as material influence significantly the magnetic reversal processes in sub-micron structured magnet. For micron and submicron wide wires both mechanisms of coherent rotation and magnetization curling are believed to be responsible for magnetization reversal. Meanwhile, several results of micro-magnetic simulation show that the complete magnetization moment rotation of an elongated particle or a planar wire is not always uniform during the reversal. Here, we have performed magnetoresistance measurements in different regions of permalloy (Py) planar wires to study the local stable magnetic configuration during the reversal process.

EXPERIMENTS

Permalloy Wires

H in plane

$L=20\mu m$, $t=30nm$
$W : 0.1 \sim 10 \mu m$
- covered by 3nm thick Au
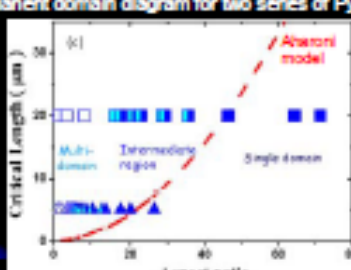- on SiN coated Si wafer

$W=0.4\mu m$

by e-beam lithography, thermal evaporation and lift-off techniques.

Four-terminal electrical transport measurement

Low frequency (15.9Hz) and low excitation current (<0.1mA).
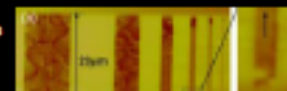Current is along the easy axis, indicated by a red arrow.

Magnetoresistance R(H,θ) at T=10K

H is in plane and makes an angle θ with the easy axis (current).
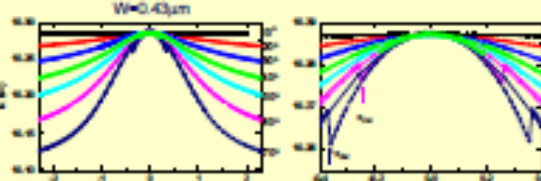
Remanent domain diagram for two series of Py planar wire.

Aharoni model

Critical Length (μm)

Multi-domain   Intermediate region   Single domain

Aspect ratio

MFM images of some Py wires at remanence after being exposed in H=1 Tesla along the easy axis

- The reversible MR is caused by the AMR effect in corporation with the coherent rotation of the magnetic moment with magnetic field.
- An irreversibly V-shaped discontinuity in low field can be clearly found for all angles θ<90°.

$W=0.43\mu m$
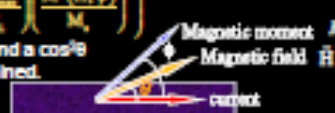
- Large reversibly bell-shaped negative MR's.

$H_{SW}(\theta)$ can be described by Aharoni model taken account for the magnetization curling.

RESULTS and DISCUSSION

For a long single domain wire, the corresponding MR based on the Stoner-Wohlfarth model with coherent rotation of magnetic reversal process is given by,
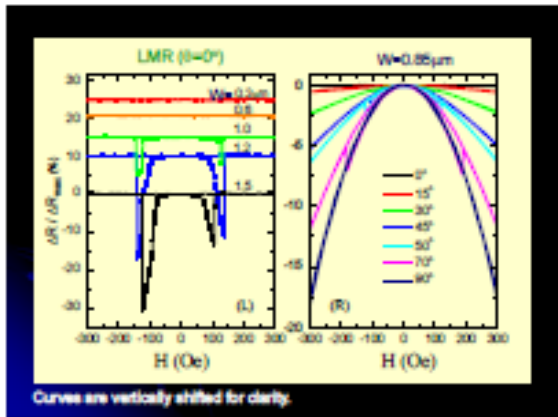
$$R(H,\theta) = R_s \left[1 + \left(\frac{\Delta R_{max}}{R_s} \right) \left(\frac{M_{\parallel}(H,\theta)}{M_s} \right)^2 \right]$$

At saturation, $\phi = \theta$ and a $\cos^2\theta$ dependence is obtained.

Magnetic moment $\vec{M}$
Magnetic field $\vec{H}$
current

$$\frac{\Delta R(H,\theta)}{\Delta R_{max}} = \frac{R(H,\theta) - R_s}{R_W - R_s}$$

R_s : the resistance at saturation w/ θ=0°
$R_\perp$: the resistance at saturation w/ θ=90°

reveals the effective percentage of deviated magnetic moments from the long axis (current).

Curves are vertically shifted for clarity.

(L) These LMR behaviors are symbolized for typical single domain wires.
- A discontinuous jump at the switch field.
- Although it is difficult to resolve the jump in the presented scale for two narrowest wires, they act like W=0.85μm shown in (R).
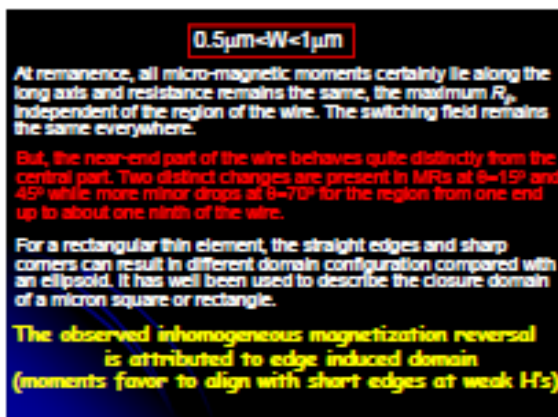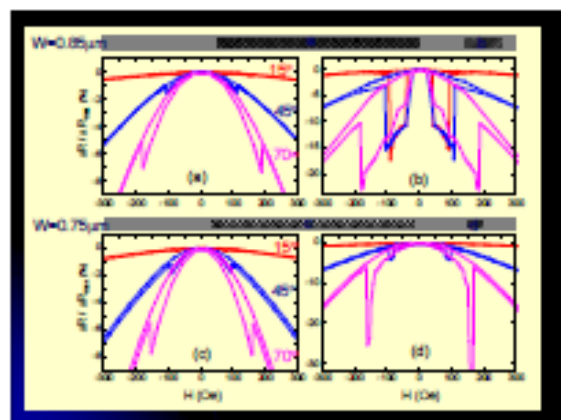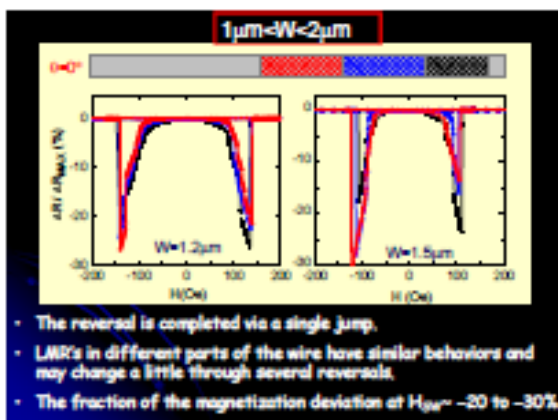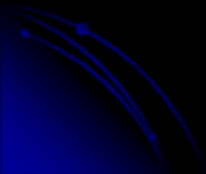 ✓ H_{sw} changes barely at low angles and increases at large angles.

Wider wires (W≥1μm) exhibit extra features upon approaching to H_{sw} in their MRs implying additional micro-magnetic domains are created during the reversal process.

- The reversal is completed via a single jump.
- LMR's in different parts of the wire have similar behaviors and may change a little through several reversals.
- The fraction of the magnetization deviation at H_{sw} ~ –20 to –30%.

At remanence, all micro-magnetic moments certainly lie along the long axis and resistance remains the same, the maximum R_p independent of the region of the wire. The switching field remains the same everywhere.

But, the near-end part of the wire behaves quite distinctly from the central part. Two distinct changes are present in MRs at θ=15° and 45° while more minor drops at θ=70° for the region from one end up to about one ninth of the wire.

For a rectangular thin element, the straight edges and sharp corners can result in different domain configuration compared with an ellipsoid. It has well been used to describe the closure domain of a micron square or rectangle.

The observed inhomogeneous magnetization reversal is attributed to edge induced domain (moments favor to align with short edges at weak H's).

A nearly homogeneous magnetization reversal spans over 95% of this wire.

Samples of width less than 0.5μm and aspect ratio larger than 40 is in the so-called "perfectly" single domain state with no vortex-like structure in both ends and no formation of domain wall during the reversal.

SUMMARY

In summary, our wires of widths in between 1.0 and 0.6μm exhibit distinct magnetization reversals in different segments. Although the central part demonstrates the typical single jump switching, two or more jumps in the MR curve occur at near-end regions. The local magnetization at the edges of the wires usually experiences additional shape anisotropy parallel to the edge and hence, both near-wire ends have the slightly complicated reversal behavior than the central region of the wire. We suggest that the near-end domain region of inhomogeneous magnetization is determined by the shape induced anisotropic constant.